



Article

# LED wristbands for Cell-based Crowd Evacuation: an Adaptive Exit-choice Guidance System Architecture

Miguel A. Lopez-Carmona \*  and Alvaro Paricio 

Departamento de Automatica, Escuela Politecnica Superior, Universidad de Alcala, Madrid, Spain;

miguelangel.lopez@uah.es (M.A.L.C.); alvaro.paricio@uah.es (A.P.)

\* Correspondence: miguelangel.lopez@uah.es; Tel.: +34-91-885-66-73

Received: date; Accepted: date; Published: date

**Abstract:** Cell-based crowd evacuation systems provide adaptive or static exit-choice indications that favor a coordinated group dynamic, improving evacuation time and safety. While a great effort has been made to modeling its control logic by assuming an ideal communication and positioning infrastructure, the architectural dimension and the influence of pedestrian positioning uncertainty have been largely overlooked. In our previous research, a Cell-based crowd evacuation system (CelleVAC) was proposed that dynamically allocates exit gates to pedestrians in a cell-based pedestrian positioning infrastructure. This system provides optimal exit-choice indications through color-based indications and a control logic module built upon an optimized discrete-choice model. Here, we investigate how location-aware technologies and wearable devices can be used for a realistic deployment of CelleVAC. We consider a simulated real evacuation scenario (Madrid Arena) and propose a system architecture for CelleVAC that includes: a controller node, a radio-controlled LED wristband subsystem, and a cell-node network equipped with active Radio Frequency Identification (RFID) devices. These subsystems coordinate to provide control, display and positioning capabilities. We quantitatively study the sensitivity of evacuation time and safety to uncertainty in the positioning system. Results showed that CelleVAC was operational within a limited range of positioning uncertainty. Further analyses revealed that reprogramming the control logic module through a simulation-optimization process, simulating the positioning system's expected uncertainty level, improved the CelleVAC performance in scenarios with poor positioning systems.

---

Crowd evacuation; LED wristbands; behavioral optimization; exit-choice decisions; simulation-optimization modeling; cell-based evacuation

## 1. Introduction

Uncoordinated crowd behaviors are known as being responsible for pedestrians' deaths and injuries in crowd evacuations. An efficient evacuation plan is crucial to direct and coordinate evacuees in a safe manner. This coordination can be achieved by deploying guidance systems that provide information for each user on the paths, the exit gates, or the evacuation start time [1].

Many algorithms have been devised for the development of evacuation guidance systems [2]. For example, network flow-based approaches model evacuation planning as a minimum cost network flow problem [3]. The main downside of network flow-based models is that evacuees must follow the paths accurately and fulfill an exact schedule. Various approaches have been suggested to solve this problem using geometric graphs [4]. For example, in [5] a wireless sensor network is partitioned into triangular areas based on the average detected temperature, and safe egress paths are calculated. Following this idea, queuing models [6] build a queuing network to estimate evacuation and congestion delays. Various approaches dynamically develop navigation paths by applying artificial potential fields to the exits and hazards [7–9]. This technique suffers from several problems, among which is the convergence time for network stabilization, and its search efficiency in scenarios with several exit gates.

There is an extensive research on biologically-inspired algorithms to search for optimal routes or recommend exits. For instance, in [10] a multiobjective evacuation route assignment model based on genetic algorithm [11,12] is proposed. In [13] bee colony optimization is used to displace evacuees to safe areas. The downside of this work is the relatively high communication overhead. A wearable device named LifeBelt is proposed in [14] that recommends exits to individuals based on the sensed environment. In [15] a shortest path algorithm computes pedestrian routes by iteratively partitioning graph edges at critical division points. Routes are iteratively refined offline until an optimal state is achieved. This approach assumes that a crowd distribution is known in advance, and does not adapt to changes during evacuation.

Since many of existing emergency response systems are built on top of Wireless Sensor Networks (WSN), routing protocols for packet transmission have been adapted to develop guidance systems in emergency scenarios. In [16] an emergency support system built on top of WSN is presented, which is inspired by the cognitive packet network routing [17] in the IoT domain. Since communications are essential in an evacuation process, opportunistic communications have also been used in the design of emergency support systems [18].

It is well known that the performance of crowd evacuation processes during emergencies can be strongly affected by exit-choice decision making at the individual level [19–21]. Thus, there are research efforts in the area of real-time guidance for crowd evacuations that have focused on studying mechanisms for providing pedestrians with optimal exit-choice information. A promising line of research in this area is that of cell-based evacuation systems [1,22,23]. These systems rely on a cell-based pedestrian positioning infrastructure such that pedestrians in a cell are assumed to receive the same exit gate instructions. In [1], a simulation-optimization framework integrates a genetic algorithm and a microscopic pedestrian simulation-assignment model. Evacuees are assumed to receive exit-choice indications that may include the optimal start time of evacuation. Similarly, in [24] the idea is to use a gene expression programming to find a heuristic rule. This rule is used to indicate people in the same sub-region to move towards the same exit. The main drawback of these approaches is that they do not consider the dynamic environment features.

Since the dynamics of the environment change over time in unpredictable ways, adaptive strategies are recognized as more adequate solutions [21]. There exist adaptive approaches of cell-based evacuation systems, in which the system's control logic module updates the cells' exit-choice indications in real-time depending on the existing environmental conditions. In [22], they propose a heuristic rule that considers the distance and width of exit doors as fixed input parameters and density around a given cell as a dynamic parameter. The crowd evacuation planning problem is converted to finding the optimal heuristic rule that minimizes the total evacuation time. To solve this problem, the authors adopt the Cartesian Genetic Programming (CGP) [25]. We developed in [23] an adaptive cell-based crowd evacuation system (CellEVAC) based on behavioral optimization that searches for the optimal evacuation plan through meta-heuristic optimization methodology. As in [22], we obtain adaptive evacuation plans capable of responding to changing environmental conditions. However, our control logic model is easier to configure and optimize, with a more straightforward logic formulation and interpretation, exhibiting a more natural pedestrian behavior.

All these approaches outlined above have mainly focused on the design of algorithms to provide optimal exit-choice indications, assuming that there exist ideal communication and pedestrian positioning infrastructures. However, for a real and effective implementation of this type of system, it is necessary to propose concrete hardware architectures whose deployment is technologically feasible at a reasonable cost. Also, given an architectural proposal, it will be essential to evaluate its influence on the performance of the evacuation processes, and if appropriate, propose corrective actions for its improvement.

In this work, we are particularly interested in proposing an adaptive cell-based evacuation system architecture using existing communication and positioning technologies, paying attention to usability, which is essential in emergency evacuations where the information of routing to exit gates should be easily interpretable. Another central question of this study concerns quantifying the influence of pedestrian positioning uncertainty in evacuation time and safety. We would also like to quantify the importance of reprogramming the control logic module under uncertainty conditions by using simulation-optimization techniques. Given a control logic optimized assuming an error-free positioning system, what would be the quantitative benefit of re-optimizing the control logic if we assume a level of uncertainty in pedestrian positioning.

With the purposes mentioned above, this paper proposes a system architecture for our adaptive cell-based evacuation system CelLEVAC [23]. The proposed system architecture consists of three subsystems: (i) monitoring and control logic subsystem, (ii) active RFID cell-node network, and (iii) radio-controlled LED wristband subsystem.

The RFID cell-node network and radio-controlled LED wristband subsystems coordinate to provide exit gate indication display and positioning capabilities to pedestrians. The monitoring and control logic subsystem monitors the environmental conditions and accordingly allocates exit gate colors to cell-nodes in real-time. Thus, the LED wristbands show the color corresponding to the cell in which each pedestrian is located, indicating the recommended exit gate.

In [23], we assumed an error-free positioning infrastructure, where pedestrians were supposed to be equipped with a generic device (smart-phone or wearable device) with ideal location-aware and color display capabilities. In this paper, the proposed positioning system's RFID communication channels are modeled using a log-normal propagation model. To define different uncertainty levels in pedestrian positioning and study its influence in evacuation time and safety, we modulate the Gaussian distribution that models the random variations in the propagation model. Finally, we apply the simulation-optimization methodology to obtain the control logic subsystem's optimal configuration under different uncertainty levels. This approach gives us information about the importance of reprogramming the control logic if we know in advance the positioning uncertainty level.

To perform simulation and simulation-optimization experiments, we have used the simulation-optimization modeling framework that we developed in [23]. This framework integrates a microscopic pedestrian simulation based on the classical Social Force Model (SFM) [26]. The simulation-optimization process adopts a Tabu-Search algorithm (TS) [27], which iteratively searches for the near-optimal evacuation plan. At the same time, the microscopic crowd simulation guides the search by evaluating the evacuation time and safety of the solutions generated by the TS algorithm.

The rest of the paper is organized as follows. Section 2 presents our proposal of system architecture for CelLEVAC, the microscopic simulation-optimization framework used to perform the experimental evaluation, and the mechanism to model positioning uncertainty. Section 3 presents the experimental evaluation and results. The last section provides concluding comments and possible research extensions.

## 2. Methods

### 2.1. Evacuation Scenario

Our evacuation scenario was *Madrid Arena*, an indoor arena located in Madrid that hosts sports events, commercial, cultural and leisure activities. It has three floors (access, intermediate, and ground) and 30,000 m<sup>2</sup>, with a capacity of 10,248 spectators. We studied the evacuation of the ground floor, which has a maximum capacity of 3,400 spectators with its retractable bleachers removed. Figure 1 shows the ground floor layout, with 1,925m<sup>2</sup> and eight exit gates (*Ex1* to *Ex8*) with widths in the range 2.5m and 6m.

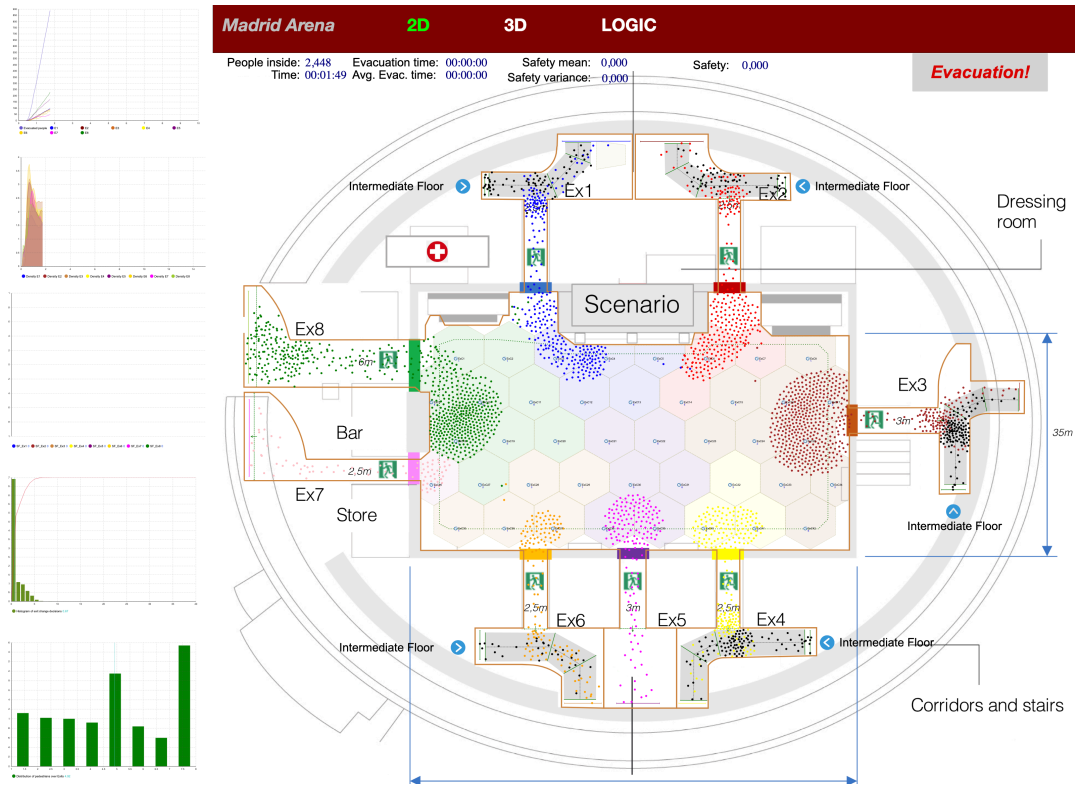


Figure 1. Madrid Arena layout (ground floor).

Pedestrian flows from intermediate floors were simulated by injecting pedestrians at exits 1, 2, 3, 4, and 6 at the entry points highlighted with a blue dot.

As in [23], we divided the ground floor into 42 regular hexagonal cells of  $9m^2$  and  $6m$  width, whose dimensions were chosen to provide a balance between control, wireless coverage, and computational efficiency.

## 2.2. System Architecture for CelLEVAC

We considered using radio-controlled LED wristbands that display colors recommending an exit gate. These LED wristbands are widely used at a range of events, from live acts at arenas to product launches, sports matches, parties, and corporate events from 1-150,000 people. The wristbands work by creating multiple flash patterns with RGB LEDs that use the full-color spectrum and can be programmed to create visual effects (Figure 2). Xylobands (<http://xyloband.com>) or CrowdLED (<https://crowdled.net>) are two examples of companies offering these kinds of products. Usually, radio control has a range of hundreds of meters, and the wristbands have a battery life of approximately 20 hours. Two extended features that can be found are the inclusion of RFID tags for registration purposes and zonal control to activate wristbands in separate groups.

Our idea was to extend the functionality of these devices, which is oriented towards creating visual effects, using them in case of emergency to guide people to color-illuminated exit gates. The displayed color in the wristband indicates the evacuee the corresponding exit gate. Besides, a synergic effect of using LED wristband lightning is that it may ease image processing for pedestrian flow estimation, which is used in our system to build the control logic.



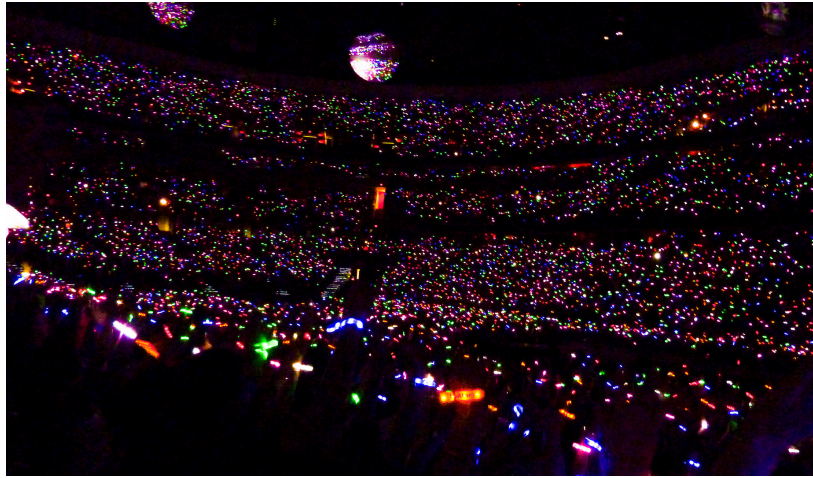


**Figure 2.** Concert of Coldplay at Verizon Center. Spectators wear LED wristbands manufactured by Xylobands (<http://xylobands.com>). Author: Matthew Straubmuller; license: <https://creativecommons.org/licenses/by/2.0/>; source: <https://www.flickr.com/photos/imatty35/7550673548>.

As described in the introduction section, the proposed system architecture consists of three subsystems:

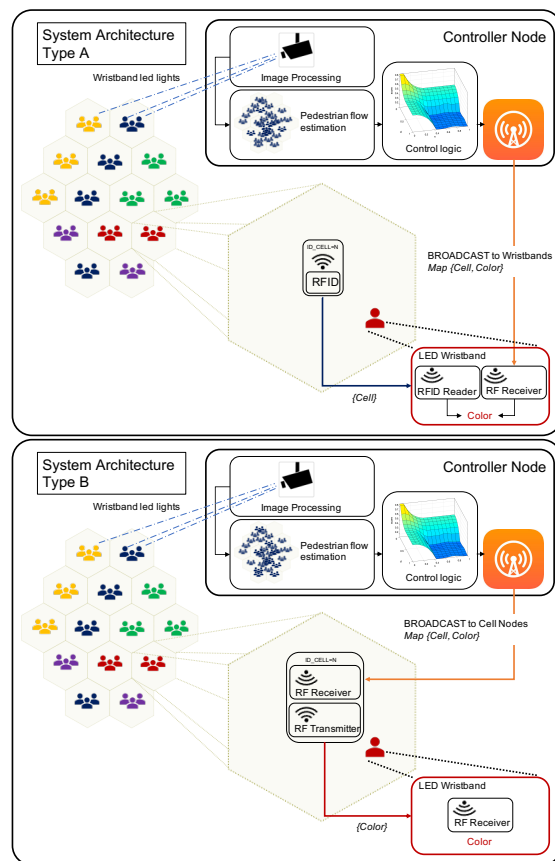
1. Monitoring and control logic subsystem (Controller Node), which monitors pedestrian flows using image processing and generates exit-choice indications in the form of color allocation to cells.
2. Active RFID cell-node network whose purpose is to provide positioning information to pedestrians' LED wristbands.
3. Radio-controlled LED wristband subsystem, which includes the LED wristbands with color display and radio-frequency (RF) communication capabilities.

Figure 3 shows two possible implementations of the system architecture (Types A and B) for deploying CelleVAC using existing off-the-shelf technologies. Both alternatives install a controller node with three functional blocks: pedestrian flow estimation based on image processing, control logic based on behavioral optimization [23], and RF transmitter.

In the controller node, the pedestrian flow estimation block performs image processing to detect LED wristbands lightning and estimate pedestrian density at each cell. In this work we assumed a flow estimation block that is based on commercially available pedestrian counting technology [28–31]. Obtained pedestrian densities feed the control logic block that computes the optimal allocation of colors to cell-nodes (see Section 2.3). The RF transmitter broadcasts messages periodically containing the 42 tuples  $\{Cell, Color\}$  that assigns a color to each cell. This process repeats every five seconds.

In the Type A architecture, each cell-node is equipped with an active RFID tag [32] that periodically broadcasts its ID (active RFID beacon [33]). On the other hand, the wristbands embed an RFID reader that reads the IDs from the surrounding cells. The wristband selects the ID of the message with the highest Received Signal Strength Indicator (RSSI) to estimate the right pedestrian location [34]. The other element in the wristband is the RF Receiver, which periodically evaluates the broadcast messages with the tuples  $\{Cell, Color\}$  from the controller node. By matching the wristband location (selected cell ID) and cell-color tuples, the wristband lights up with the exit gate color assigned to the cell.

In the Type B architecture, the RF Receiver in the cell-node receives the broadcast messages from the controller node with the assigned color. Then, the cell-node broadcasts the corresponding color message, which is read by the wristbands. As in the Type A architecture, several broadcast messages from different



**Figure 3.** CellEVAC System Architecture: Types A and B.

cell-nodes can be received within a window time. So, the same signal strength selection mechanism is used by the wristbands to select the right color.

The most critical part of this architecture is in the positioning functionality. Both RFID and RF communication channels between the cell-node network and wristbands have to cope with a complex signal propagation environment. However, the system does not need to obtain exact position coordinates but select the right cell in which the pedestrians are located. It means that a significant lower location resolution is needed and that there is no need to implement triangulation mechanisms based on RSSI [35]. Another problem to solve is co-channel interference, which may be managed using existing radio resource management schemes [36]. Besides, the RF transmission channel in the controller node is a one-to-many communication channel that has been used to control commercially available LED wristbands in large events for more than a decade, and do not pose a particular challenge.

### 2.3. Control Logic of CelleVAC

The control logic of CelleVAC is based on a behavioral optimization approach proposed in our previous work in [23]. Here we recall the main concepts that build its operation.

Pedestrians' exit-choice decision modeling based on discrete choice theory [37] inspired the control logic developed for CelleVAC. Thus, we modeled exit gate color allocation to cell-nodes using the simplest and most popular practical discrete choice model, the Multinomial Logit Model (MLM) [37,38]. In the MLM control logic, the controller node allocates exit gates (colors) to cells using a probabilistic model, in which the allocation probabilities of exit gate  $j$  to cell-node  $c$  are given by:

$$P_{cj} = \frac{\exp(V_{cj})}{\sum_{E_i \in E(c)} \exp(V_{ci})} \quad (1)$$

where  $E = \{E_{i=1...42}\}$  is the set of exit gates, and  $V_{cj}$  is the systematic utility function for cell  $c$  and exit gate  $j$ , which is given by:

$$\begin{aligned} V_{cj} = & \beta_D \times \frac{DISTANCE_{cj}}{\max(DISTANCE)} + \beta_W \times \frac{WIDTH_j}{\max(WIDTH)} \\ & + \beta_G \times \frac{GROUP_{cj} - GROUP_{min}}{GROUP_{cj}} + \beta_E \times \frac{EXCON_j}{criticalDensity_j} \\ & + \beta_C(t) \times NOCHANGING_{cj} \end{aligned} \quad (2)$$

The first attribute is the distance from cell-node  $c$  to exit gate  $j$ , while the second attribute represents the width of each exit gate. Both attributes are normalized in the range of 0-1.

The third attribute is the *GROUP* ratio, which estimates the congestion along a path from cell  $c$  to an exit gate  $j$ , relative to the least congested path. A group ratio value of 0 indicates that the chosen path is the least congested. When the value of the group ratio tends towards 1, it means that the emptiest path's imbalance becomes large. The parameter  $\beta_G$  is expected to be positive if it favors pedestrians to follow other pedestrians and is negative otherwise. Note that with this normalization, we assume that the attribute's relevance is kept constant throughout the evacuation process.

The fourth attribute *EXCON* accommodates the congestion at exit gates. For a given density value, congestion is higher if the pedestrian flow is low. We reflect this effect through critical density values obtained from the fundamental diagrams of each exit gate (see [23]). This *criticalDensity<sub>j</sub>* value reflects the

density value at which the exit gate's maximum capacity is reached. Therefore, the  $EXCON_j$  value representing density at exit gate  $j$  is normalized by the corresponding  $criticalDensity_j$  value. This normalization converts  $EXCON$  into a unitless attribute around 1. When the value of  $EXCON$  is above 1, it means that exit is highly congested. A value close to 0 would indicate that the exit gate is almost empty. In contrast to the normalization procedure used for the  $GROUP$  attribute, the distribution of  $EXCON$  values exhibits a decreasing evolution as the number of pedestrians in the evacuation scenario decreases. It seems reasonable to assume that the relevance of congestion at exits as a discriminant factor for exit-choice decreases when the overall number of pedestrians is low, and so  $EXCON$  is close to 0 at all exits.

The fifth attribute is the  $NOCHANGING$  value associated with cell-node  $c$  and exit  $j$ , which captures how the controller is likely to revise the previous exit gate allocation (this attribute was named  $PERSONAL$  in [23]). We treat this attribute as a binary categorical 0-1 value that equals 1 if the current exit gate of cell  $c$  is  $j$ , and is 0 otherwise ( $NOCHANGING = 0 \forall k \neq j$ ). Therefore, in a general context, the parameter  $\beta_C(t)$  is expected to be positive if the controller tends to maintain the previous exit gate allocations, and is negative otherwise. However, we aimed to modulate the tendency to maintain previous decisions, and so,  $\beta_C(t)$  is always positive. As was noted above, we assumed that exit-choice changing evolves as evacuation progresses, and therefore the parameter that modulates  $NOCHANGING$  is time-dependent. By observing the pattern of behavior under various simulation settings, it was found reasonable that the tendency to maintain decisions increased linearly depending on the current number of pedestrians:

$$\beta_C(t) = \beta_C \times \left( 1 - \frac{numOfPeds(t)}{numOfPeds(t=0)} \right) \quad (3)$$

According to Equation 3, the parameter  $\beta_C(t \rightarrow 0)$  tends to 0 at the beginning of the evacuation, and so, the tendency to revise decisions is higher. As the number of pedestrians decreases, the parameter  $\beta_C(t)$  tends to  $\beta_C$ , and the tendency is to maintain previous decisions proportionally to the  $\beta_C$  value.

In the simulation setting used in this work, we used an update cycle of 5 seconds. We kept this frequency constant and controlled the frequency of the changes at optimal levels using the parameter  $\beta_C$ .

#### 2.4. Modeling Positioning Uncertainty

Active RFID systems are defined by three parts, a reader (wristband), antennas, and a tag (cell-node), with their power source. In active RFID applications, RSSI can be used for determining the location of a tag, such that each tag's RSSI value is proportional to the distance. In our system, the cell-node embeds an active beacon tag that sends out its ID every 3 - 5 seconds. Thus, each tag's RSSI value is proportional to the distance between the wristband and cell-node. However, the RSSI value in active RFID applications can be affected by multipath and signal collision [35].

In free-space, the relationship of the power transmitted from cell-node to wristbands, assuming the antennas are isotropic and have no directivity, is expressed by the free-space path loss equation derived from the Friis transmission equation:

$$PL(dB) = 20 \log_{10}(d) + 20 \log_{10}(f) - 27.55 \quad (4)$$

where  $PL$  is the free-space path loss in dB,  $f$  is the signal frequency in MHz, and  $d$  is the distance in meters from the cell-node to the wristband. For converting RSSI values into a distance measurement in indoor environments with random shadowing effects, one of the most common approaches taken is to use the log-normal propagation model [39,40]:

$$P_{RX_{dBm}} = RSSI = P_{TX_{dBm}} - PL_0 - 10\eta \log_{10} \frac{d}{d_0} + X_g \quad (5)$$

where  $P_{TX_{dBm}}$  is the transmitted power in  $dBm$ ,  $P_{RX_{dBm}}$  is the received power,  $PL_0$  is the path loss for a reference distance  $d_0$  calculated using the free-space path loss equation (Equation 4) or by field measurements,  $d \geq d_0$  is an arbitrary distance,  $\eta$  is the path loss exponent, and  $X_g$  is a gaussian random variable with zero mean and variance  $\sigma^2$  that models the random variation of the RSSI value. The path loss exponent  $\eta$  in indoor environments such as stadiums can reach values in the range of 4 to 7.

User preference or environmental considerations usually prescribe which parameter configuration to use for most applications. In our simulation scenario, we used a frequency of  $2.45GHz$ , transmission power of  $10W$ , path loss exponent  $\eta = 5$ , and reference distance  $d_0 = 1m$ . Thus, RSSI can be expressed as

$$RSSI = -60 \log_{10}(d) + X_g, d \geq 1m \quad (6)$$

Modifying the variance  $\sigma_g^2$  of the gaussian distribution  $X_g$  we may modulate positioning uncertainty.

The procedure to calculate each pedestrian's location in evacuation simulations is a two-step process that repeats every five seconds:

1. Given the set of cell-nodes  $\{c_{i=1...42}\}$  obtain the set of distances  $\{d_{i=1...42}\}$  from pedestrian to each cell-node  $c_i$ , and calculate the corresponding set  $\{RSSI_i\}$  using Equation 6.
2. If there exists a distance value  $d_i$  in set  $\{d_{i=1...42}\}$  such that  $d_i < 1m$ , the pedestrian location is  $c_i$ . Otherwise, the pedestrian location corresponds to the cell  $c_i$  with the maximum  $RSSI_i$  value.

## 2.5. Microscopic Simulation-optimization Framework

Much of the related work on crowd evacuations rely on detailed simulations. We opted for a multi-agent microscopic simulation framework based on a Social Force Model (SFM) [26] due to its flexibility and ease of integration of complex interaction and behavior models. Our simulation framework integrates the potential of SFM to mimic physical interactions among evacuees, and of multi-agent systems to simulate complex behaviors and interactions [41].

In this work, the simulation-optimization software framework we developed in [23] has been extended with the positioning uncertainty model. The software framework embeds agent-based simulation and discrete event simulation, integrating pedestrian behavior modeling, SFM for pedestrian motion, control logic of exit gate indications, positioning, and optimization features.

We used the commercially available programming, modeling and simulation software packages AnyLogic<sup>1</sup> and Matlab<sup>2</sup>. The kernel of the simulation-optimization software framework is AnyLogic, which integrates three different modeling methods: discrete event simulation, agent-based simulation, and system dynamics, built on top of a Java-based software development framework. The evacuation scenario layout, pedestrian motion, and evacuation measurements run in AnyLogic, while exit-choice decisions and control logic of exit gate indications are implemented in Matlab. AnyLogic and Matlab are interconnected in a master-slave configuration through the interface with external Java libraries provided by AnyLogic and the Matlab Java API engine (see details below).

The CelleVAC simulation model with MLM control logic is shown in Figure 4. The evacuation scenario layout, visualization features, and all the functionality regarding the SFM based pedestrian motion were implemented within AnyLogic.

During a simulation, the first step is to send from AnyLogic to Matlab the set of parameters that configure the CelleVAC MLM and Pedestrians' positioning modules, including the set of cell-node center

<sup>1</sup> <https://www.anylogic.com/> Accessed 18 August 2020

<sup>2</sup> <https://www.mathworks.com/> Accessed 19 June 2020



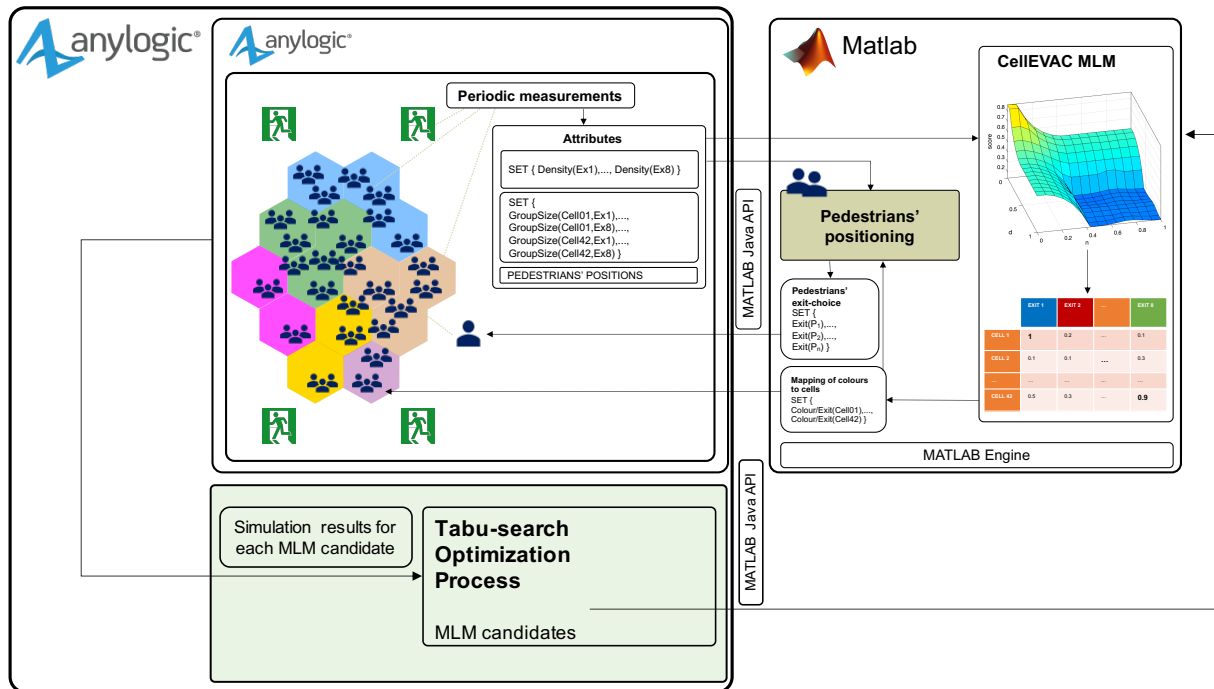


**Figure 4.** Simulation-optimization software framework of CellEVAC with control logic based on Multinomial Logit Model (MLM).

coordinates and exit gates, and the uncertainty level. Next, the pedestrian positioning and densities at exit gates and cells are periodically measured and then transformed into the set of attributes: pedestrian positions, density at each exit gate, and group of pedestrians along the path to each exit. The group size of each pair cell-exit gate is calculated by adding the pedestrians in the cells that are closer to each exit. All these attributes feed the CellEVAC MLM module in Matlab that implements the decision logic to map colors (exit gates) to cells. This mapping is sent back to AnyLogic for visualization purposes, and to the Pedestrians' positioning module within Matlab to allocate exit gates (colors) to pedestrians (LED wristbands). The Pedestrians' positioning module implements the function that locates each pedestrian in a given cell-node using the positioning uncertainty model. The output of the Pedestrians' positioning module is the set of pairs pedestrian-exit gate, which is sent to AnyLogic for simulating pedestrian motion.

To search for optimal configurations of the MLM model, we used a simulation-optimization process that adopts a Tabu-Search algorithm (TS) [27], which iteratively searches the solution space. At the same time, the microscopic crowd simulation guides the search by evaluating the evacuation time and safety of the solutions generated by the TS algorithm. The optimization process is built on top of the OptQuest<sup>3</sup> optimization engine provided by AnyLogic. Figure 4 shows the optimization module on a green background. The parameters of the CellEVAC MLM model are the "MLM candidates" generated by the TS algorithm. Thus, each candidate is defined by a tentative set of parameters  $\beta$  sent to the MATLAB Engine at each iteration of the optimization process. The simulations results are sent back to the optimization module for its evaluation and thus guide the optimization process.

<sup>3</sup> <https://www.opttek.com/> Accessed 18 August 2020

### 3. Simulation-optimization Experiments and Results

The performance measurements in all the experiments were the *total evacuation time*, *average safety*, *variance of safety*, and the *average number of pedestrians' exit-choice decision changes*. The average and variance of safety are based on the safety values computed at the different exit gates. Average safety characterizes the overall safety value, while the variance of safety is used to estimate the imbalance of safety between the exit gates. The procedure to calculate exits' safety values is first to obtain their Fundamental Diagrams (FD) derived through microscopic simulation. The FD represents the relation between pedestrians' flow and density. Given the FDs, a procedure is defined to obtain three density thresholds. These density thresholds and the measurements of density during an evacuation process are used to calculate the safety values. For a detailed description of how we modeled pedestrian flows and safety, see [23]. In this paper, we used the same thresholds and parameters defined in [23] to measure the safety values.

We conducted two types of experiments: (i) sensitivity analysis to positioning uncertainty, and (ii) simulation-optimization. In all the simulation setups, the evacuee population consisted of 3400 pedestrians on the ground floor, who had a preferred evacuation speed obtained from a uniform distribution between 1.24 and 1.48  $m/s$ . To speed up the simulation-optimization experiments, we imposed a deadline of 25 minutes to each evacuation simulation iteration, after which the simulation iteration was aborted.

Two different evacuation scenarios were considered depending on the experiment: evacuations without external flows (NEF) in which no pedestrians were coming from the upper floors, and evacuations with external flows (EF) (i.e., with pedestrians coming from the upper floors) to simulate more complex pedestrian flow interactions. In EF scenarios, three exit gates were chosen at random at each simulation iteration. Two of these exit gates received an incoming pedestrian flow rate of 120  $peds/m$ , while the third exit gate was blocked.

In the sensitivity analysis experiments, each experiment ran the evacuation simulation model multiple times varying the positioning uncertainty level (variance of the Gaussian distribution  $X_g$ ), showing how the simulation output (i.e., the performance measurements) depended on it. Due to the stochastic nature of the evacuation processes, we used a replication algorithm to obtain representative results for a given parameter setting and a specific simulation output. This algorithm defines a minimum and a maximum number of experimental runs per parameter setting (replications of a simulation), a confidence level for the sample mean of replications (simulation output average), and an error percent. The minimum number guarantees the minimum number of replications, while the confidence level and error percent determine if more replications are needed. Simulations for a given parameter configuration stops when the maximum number of replications has been run or when the confidence level is within the given percentage of the mean of the replications to date. In our experimental setup, evacuation time was used as an output parameter to control the number of replications between 10 and 50. The confidence level was fixed to 95%, and the error percent to 0.5.

In the simulation-optimization experiments, we used the Tabu-search optimization algorithm [27]. The goal was to find the optimal combination of parameters of the MLM model that resulted in the best possible solution. We considered two different optimization scenarios characterized by the fitness function (objective function) used and the existence of external pedestrian flows.

- **NEF:** Optimize Time and Safety ( $\min(evacTime - Sf)$ ) without External Flows. The goal is to optimize evacuation time and average safety, and the evacuation scenario does not include external pedestrian flows.
- **EF:** Optimize Time and Safety ( $\min(evacTime - Sf)$ ) with External Flows. The goal is to optimize evacuation time and average safety, and the evacuation scenario includes external pedestrian flows.

As in the sensitivity analysis experiments, the optimization algorithm applies a replication algorithm. However, while in the sensitivity analysis, the number of replicas was limited by the evacuation time

**Table 1.** Optimal parameter configuration for the CelleVAC MLM decision logic model, and parameter configuration of the MLM pedestrians' standard behavior model.

	$\beta_D$	$\beta_G$	$\beta_E$	$\beta_W$	$\beta_C$
Optimal CelleVAC for 0dB	-17.723	-2.181	-1.671	1.064	2.594
Standard (without CelleVAC)	-28	0.6	-0.5	0.6	0

value, in simulation-optimizations, the stop condition was controlled by the fitness function (objective function).

### 3.1. Sensitivity Analysis of Positioning Uncertainty

In the sensitivity analysis of evacuation performance to positioning uncertainty, the standard deviation  $\sigma_g$  in  $X_g$  (Equation 6) was varied from 0dB to 40dB at discrete steps in two different evacuation scenarios, with and without external pedestrian flows. To evaluate up to which uncertainty level is beneficial CelleVAC in comparison with not using a guidance system, we also included the case in which pedestrians did not use the CelleVAC system (coded as  $\sigma_g = N$  in the result box-plots). The optimal parameter configuration of the MNL model found in [23] was used to implement the CelleVAC decision logic (Table 1). For the experiments in which pedestrians did not use CelleVAC, the decision logic was implemented at a pedestrian level using the configuration of parameters of the MLM model defined in [23] that simulates standard pedestrian behavior.

For illustration purposes, Figure 5 shows still images 25 seconds after the start of the evacuation for different standard deviation values  $\sigma_g$ , from 0dB to 40dB. As expected, the snapshots exhibited a progressive level of error in cell detection, becoming more evident from 15dB.

In evacuation scenarios without external flows (Figure 6), results revealed that evacuation time increased linearly for  $\sigma_g$  above 5dB. Regarding safety, increasing values of  $\sigma_g$  had a significant negative impact on average safety, though for  $\sigma_g$  above 10dB average safety stabilized around  $-15$ . Besides, the impact on safety variance was not so significant as in average safety. As expected, performance worsened for increasing  $\sigma_g$ , though for values above 20dB safety variance tended to improve and stabilize. At the cost of an increasing evacuation time, we observed how uncoordinated pedestrians' movement when positioning uncertainty was high, made spatial-density at exit gates decrease, and so safety measurements stabilize or improve. The number of exit-choice decision changes increased exponentially with  $\sigma_g$ , due to the logarithmic scale (dB) used to define the values of  $\sigma_g$ .

When compared to evacuations without external flows in which CelleVAC did not operate, and not considering the safety variance, we observed that using CelleVAC was beneficial strictly for values of  $\sigma_g$  below 5dB. Higher values of  $\sigma_g$  could be valid at the cost of an increase in evacuation time. However, note that not using CelleVAC comes at the cost of a significantly higher safety variance.

In evacuation scenarios with external flows, the sensitivity analysis results revealed the same trend as without external pedestrian flows (Figure 7). When compared to evacuations that did not use CelleVAC, and not considering the safety variance, the benefit of CelleVAC expanded to  $\sigma_g$  below 10dB. However, note that safety variance is exceptionally high when not using CelleVAC, which means that pedestrian flows at different exit gates is highly unbalanced.

Overall, the results of the sensitivity analyses for scenarios with and without external flows suggest a clear benefit of using CelleVAC if the positioning system exhibits RSSI random variations below 10dB.

### 3.2. Optimizing CelleVAC for Different Positioning Uncertainty Levels

Figure 8 shows the progress of the Tabu-search simulation-optimization of the MLM models' parameter configurations for values of  $\sigma_g$  equal to 5, 15 and 20dB. The objective was to optimize

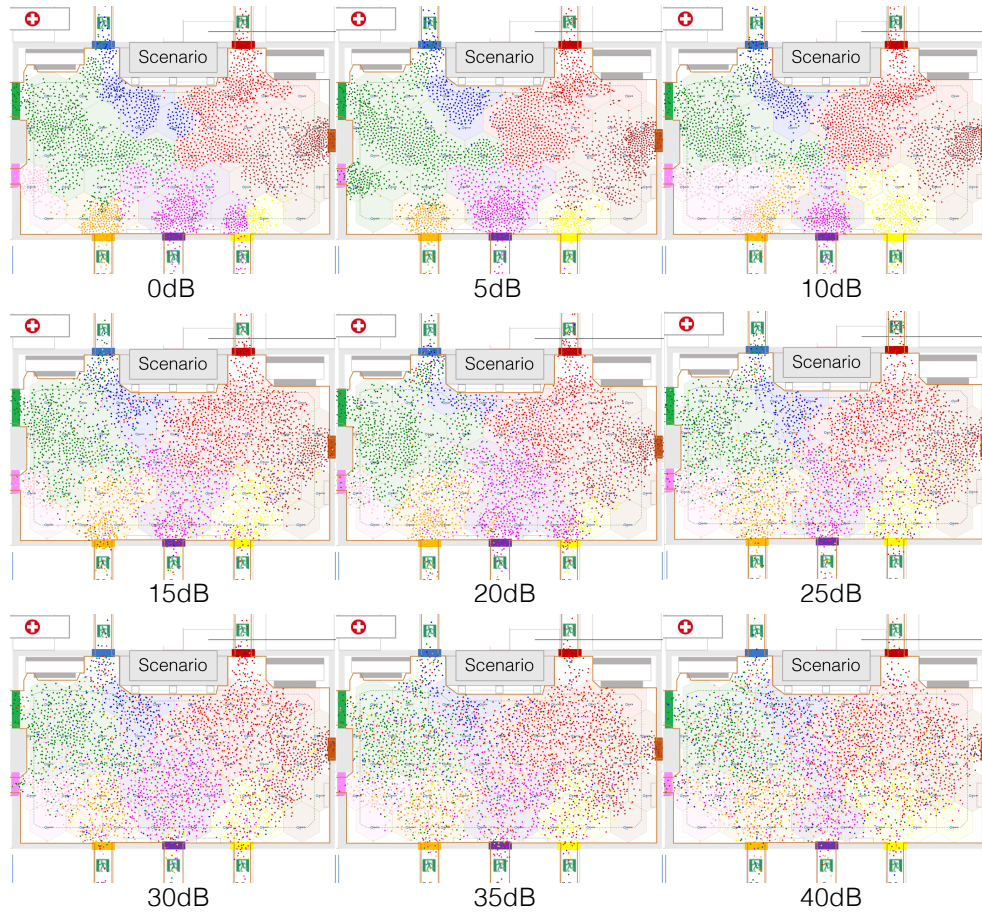


**Figure 5.** Still images 25 seconds after the start of the evacuation from single run simulation experiments for different standard deviation values  $\sigma_g$ . The cells are shaded with the exit-gate color allocated by the controller node. Colored dots represent pedestrians with the colors shown by their LED wristbands.

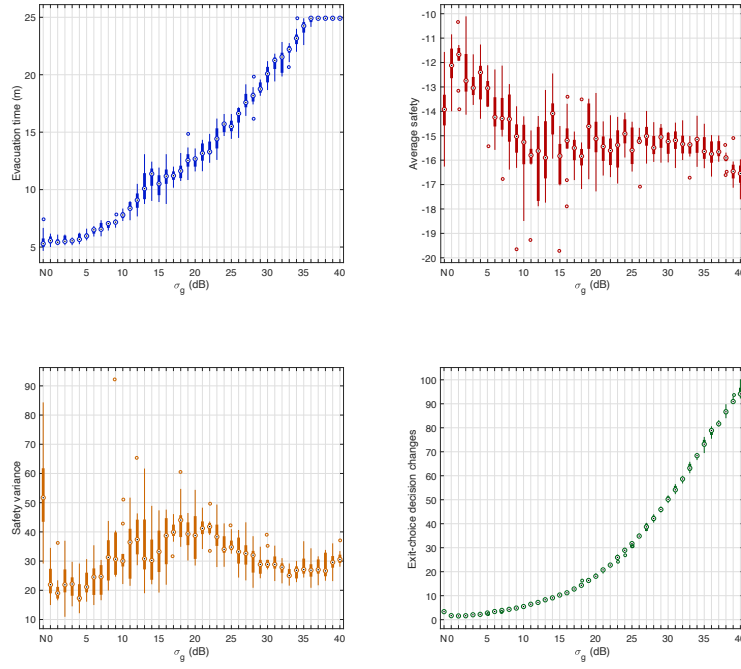


**Figure 6.** Sensitivity analysis of the positioning uncertainty in evacuation scenarios without external pedestrian flows. The box-plots on the first row show the sensitivity of evacuation time and average safety to standard deviation values  $\sigma_g$  in the range 0dB to 40dB. The second-row plots show the sensitivity of safety variance and the number of decision changes to the standard deviation values  $\sigma_g$ . In the four box-plots,  $\sigma_g = N$  represents an evacuation scenario in which pedestrians do not use Cellevac.

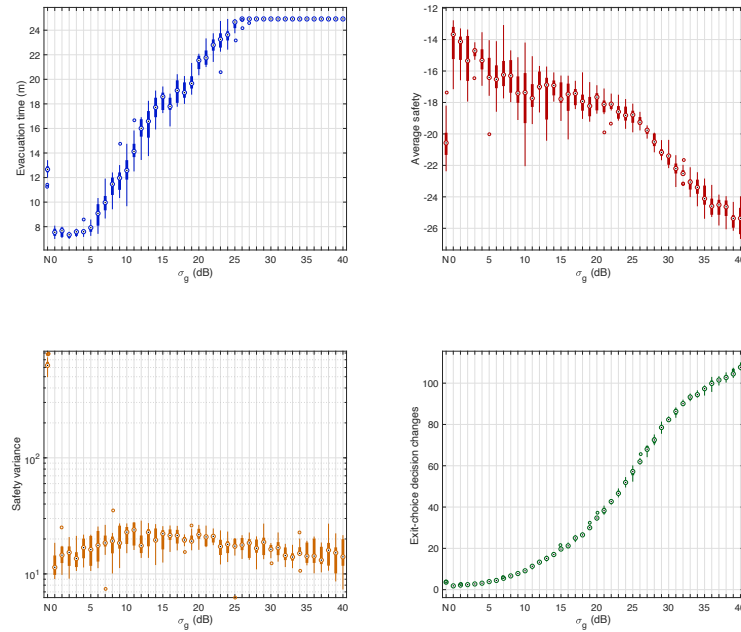


**Figure 7.** Sensitivity analysis of the positioning uncertainty in evacuation scenarios with external pedestrian flows. The box-plots on the first row show the sensitivity of evacuation time and average safety to standard deviation values  $\sigma_g$  in the range 0dB to 40dB. The second-row plots show the sensitivity of safety variance and the number of decision changes to the standard deviation values  $\sigma_g$ . In the four box-plots,  $\sigma_g = N$  represents an evacuation scenario in which pedestrians do not use Cellevac.



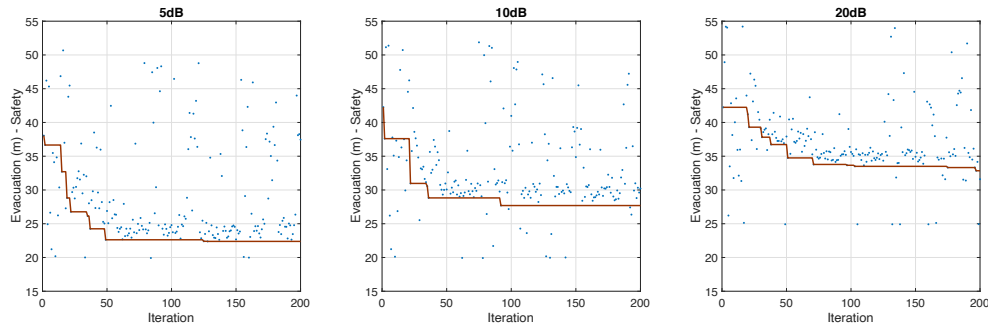


**Figure 8.** Progress of the Tabu-search simulation-optimization of the MLM models that implement the CelLEVAC guidance system for  $\sigma_g$  equal to 5, 15 and 20dB. Solutions below the current best solution (red line) correspond to non-viable solutions.

**Table 2.** Optimal parameter configurations of the MLM model for different values of  $\sigma_g$ .

$\sigma_g$	$\beta_D$	$\beta_G$	$\beta_E$	$\beta_W$	$\beta_C$
0dB	-17.723	-2.181	-1.671	1.064	2.594
5dB	-16,040	-3,224	-2,267	0	6,816
10dB	-17.696	-2	-2	1.685	3
20dB	-28.479	10	-3.083	0.041	4.025

evacuation time and average safety in scenarios with external flows. It was assumed that the entire population of evacuees followed the indications of the CelLEVAC system. Also, we imposed an arbitrary simulation stop-limit of 25 minutes to evacuation time, and a restriction to the viability of the solutions was incorporated to remove solutions in which there were pedestrians pending evacuation.

The optimal parameter configurations found are shown in Table 2. We did not observe significant differences between the different parameter configurations, except for the  $\beta_D$  and  $\beta_G$  parameters. The distance parameter gained more influence in scenarios with high positioning uncertainty. Remarkably, for  $\sigma_g = 20\text{dB}$ , the group parameter  $\beta_G$  had a positive sign. Our interpretation is that a higher influence of distance and a positive value of  $\beta_G$  contributes to more uniformity in the exit gate indications and less scattering in color allocation to cells. As a consequence of this, the probability of location error decreases.

The optimal configurations found were tested in evacuations with different positioning uncertainty levels, from 0dB to 40dB in steps of 5dB. The results have been summarized in Figures 9 and 10 under evacuation scenarios without and with external flows, respectively.

In evacuation scenarios without external flows (Figure 9), average evacuation time, and exit-choice decision change performance measurements did not show significant differences between the different configurations and evacuation scenarios. Interestingly, we found a positive trend in the results in terms of average safety and safety variance for evacuation scenarios for 20dB and above when using the optimal configuration found for 20dB. In evacuation scenarios with external flows (Figure 10), the results were similar except for safety variance, for which we did not observe any improvement.

The results presented in section 3.1 show that CelLEVAC is useful only if the positioning system exhibits RSSI random variations below 10dB. Besides, the performance analysis results of the optimal configurations do not exhibit any improvement below 20dB. Consequently, we can conclude that there is no evidence that optimizing the MLM model under the assumption of an expected random variance of RSSI contributes to an improvement in the performance of the CelLEVAC system.

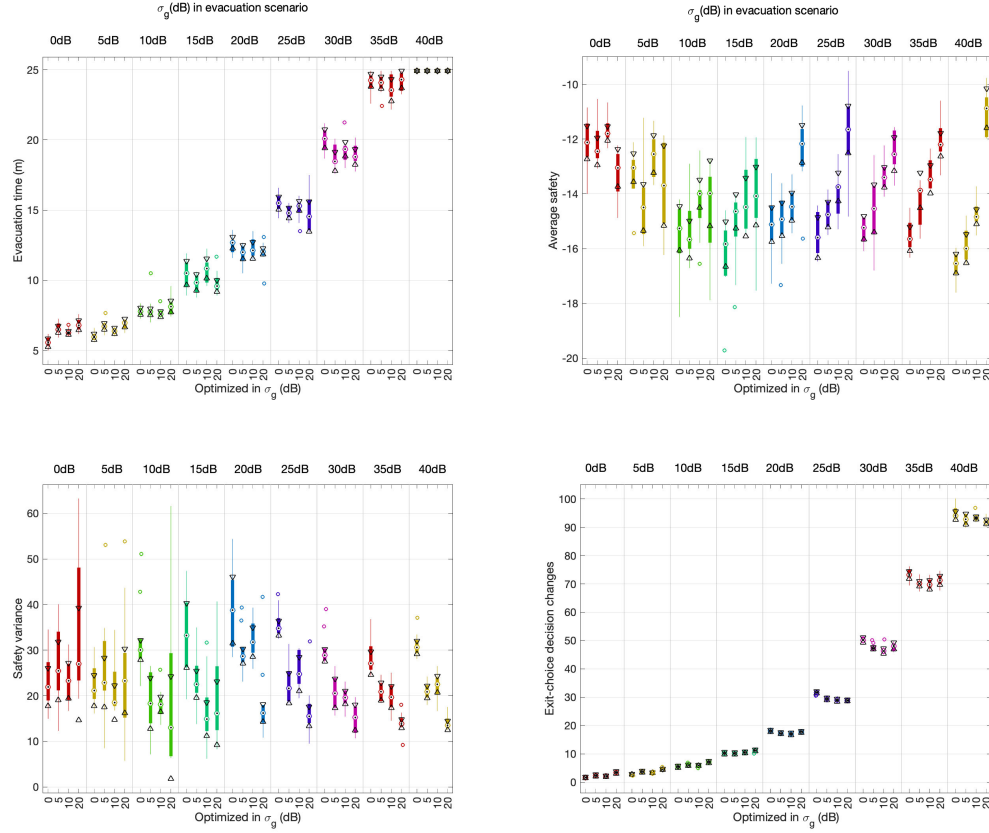


**Figure 9.** Median box-plots of the performance measurements of the optimal configurations of CelleVAC for  $\sigma_g = 0, 5, 10, 20$  dB, in evacuation scenarios without external pedestrian flows and with positioning uncertainty levels from 0 dB to 40 dB in steps of 5 dB. Bottom horizontal axes categorize the optimal configuration of parameters used (0, 5, 10, or 20 dB) to configure CelleVAC. Upper horizontal axes categorize the  $\sigma_g$  value that models the positioning system in the evacuation scenario. For instance, a value of 25 dB in the axis “ $\sigma_g$  (dB) in evacuation scenario” and 15 dB in “Optimized in  $\sigma_g$  (dB)” expresses that CelleVAC has been configured to use the optimal configuration found with 15 dB, and that it is tested in an evacuation scenario with  $\sigma_g = 25$  dB. The triangles in the box-plots display the variability of the median between samples. If the notches of two measurements do not overlap, they have different medians at the 5% significance level.

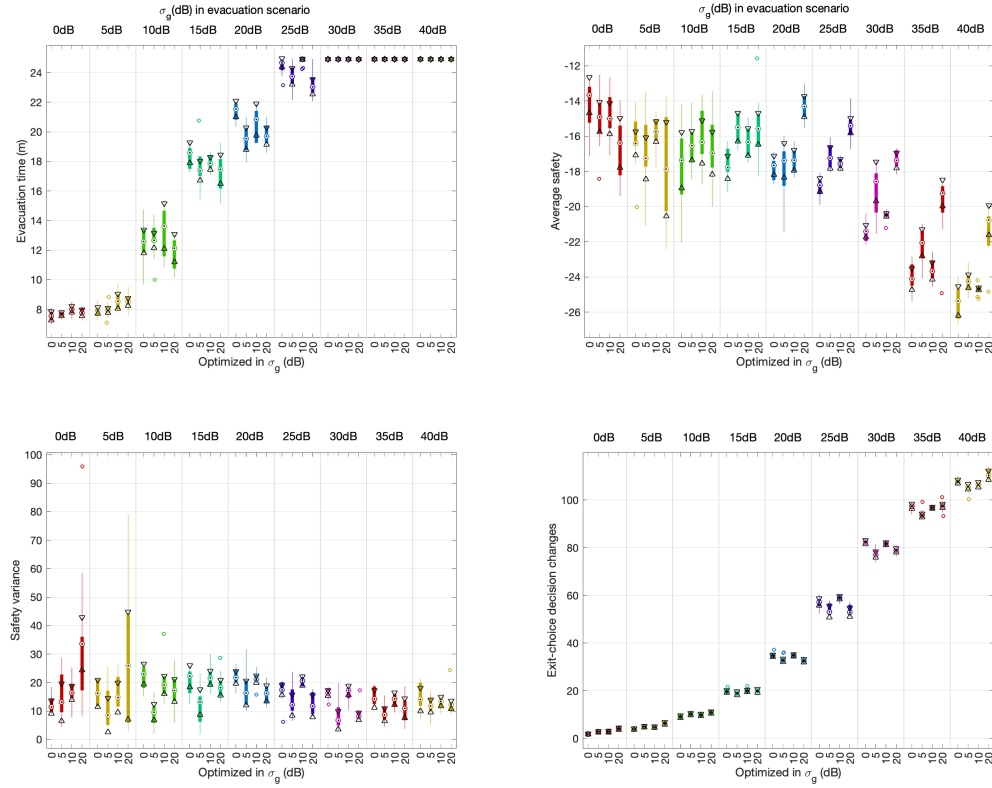


**Figure 10.** Median box-plots of the performance measurements of the optimal configurations of CelleVAC for  $\sigma_g = 0, 5, 10, 20$  dB, in evacuation scenarios with external pedestrian flows and with positioning uncertainty levels from 0 dB to 40 dB in steps of 5 dB. Bottom horizontal axes categorize the optimal configuration of parameters used (0, 5, 10, or 20 dB) to configure CelleVAC. Upper horizontal axes categorize the  $\sigma_g$  value that models the positioning system in the evacuation scenario.

#### 4. Conclusion

Our use of an MLM model to implement the control logic of Cell-based crowd evacuation systems has proven to be very efficient (see [23]). However, as in other existing works on cell-based crowd evacuation systems [1,15,24], little attention has been paid to propose a system architecture based on existing technologies and assuming real communication and positioning infrastructures. In our opinion, these considerations are crucial to boost the real implementation of these systems.

In this paper, we have proposed a specific system architecture built upon radio-controlled LED wristbands that connect with a cell-node network and a controller node, through radio-frequency communication channels. The use of LED wristbands has numerous advantages, among which we highlight its low cost, being a technology widely used to create visual effects at large events, and being an intuitive and straightforward interface that can make it exceptionally efficient in emergencies. This type of indication system greatly simplifies the interpretation of exit gate indications, which is particularly important in stressful situations found typically in evacuation scenarios. Indirectly, it can also improve the accuracy of the detection of pedestrian flows in the controller node.

Another of our aims was to quantitatively study the sensitivity of evacuation time and safety to uncertainty in the positioning system. With this objective, we have modeled the communication channel between the LED wristbands and the cell-nodes using a log-normal propagation model. To model different levels of uncertainty in positioning, we have modulated the random variations of RSSI from the propagation model. In the sensitivity analysis of performance parameters to different values of RSSI variance, CelleVAC is shown to be operational strictly up to values of 10dB. The system generates too many color changes in the wristbands and a significant increase in evacuation times for higher values.

Our last goal was to evaluate if it was possible to improve the CelleVAC performance obtaining new optimal MLM parameter configurations in which different levels of RSSI standard deviation were assumed. The results obtained have revealed that improvements found are relevant only for evacuation scenarios with levels of positioning uncertainty greater than 20dB, in which CelleVAC is not operational. Thus, to optimize the MLM model used in the CelleVAC control logic, it is valid to assume that the positioning system is error-free. However, the system cannot be applied in a real environment if the standard deviation of the RSSI values is greater than 10dB.

Several extensions are being considered for this research, mainly focused on investigating how to expand the allowed range of RSSI variation without the need to modify the existing positioning infrastructure. Another research extension is related to developing a prototype of the CelleVAC system architecture proposed in this paper.

**Author Contributions:** Conceptualization, M.A.L.C.; methodology, M.A.L.C and A.P.; software, M.A.L.C.; validation, A.P. and M.A.L.C.; investigation, M.A.L.C and A.P.; resources, M.A.L.C; data curation, M.A.L.C and A.P.; writing—original draft preparation, M.A.L.C.; writing—review and editing, M.A.L.C and A.P.; visualization, A.P. and M.A.L.C; supervision, M.A.L.C; project administration, M.A.L.C; funding acquisition, M.A.L.C.

**Funding:** This work was supported in part by the Spanish Ministry of Economy, Industry, and Competitiveness under Grant TIN2016-80622-P (AEI/FEDER, UE).

**Conflicts of Interest:** The authors declare no conflict of interest.

1. Abdelghany, A.; Abdelghany, K.; Mahmassani, H.; Alhalabi, W. Modeling Framework for Optimal Evacuation of Large-Scale Crowded Pedestrian Facilities. *European Journal of Operational Research* **2014**, *237*, 1105–1118. doi:10.1016/j.ejor.2014.02.054.
2. Bi, H.; Gelenbe, E. A Survey of Algorithms and Systems for Evacuating People in Confined Spaces. *Electronics* **2019**, *8*, 711. doi:10.3390/electronics8060711.

3. Ford, L.R.; Fulkerson, D.R. *Flows in Networks*; Princeton University Press, 1962.
4. Li, X.; Calinescu, G.; Wan, P.J.; Wang, Y. Localized Delaunay Triangulation with Application in Ad Hoc Wireless Networks. *IEEE Trans. Parallel Distrib. Syst.* **2003**, *14*, 1035–1047. doi:10.1109/tpds.2003.1239871.
5. Chen, P.Y.; Chen, W.T.; Shen, Y.T. A Distributed Area-Based Guiding Navigation Protocol for Wireless Sensor Networks. 2008 14th IEEE International Conference on Parallel and Distributed Systems, 2008, pp. 647–654. doi:10.1109/ICPADS.2008.80.
6. Newell, C. *Applications of Queueing Theory*; Vol. 4, Springer Science & Business Media, 2013.
7. Koditschek, D. Robot Planning and Control Via Potential Functions. *The Robotics Review* **1989**, pp. 349–367.
8. Hill, J.; Szewczyk, R.; Woo, A.; Hollar, S.; Culler, D.; Pister, K. System Architecture Directions for Networked Sensors. Proceedings of the Ninth International Conference on Architectural Support for Programming Languages and Operating Systems; ACM: New York, NY, USA, 2000; ASPLOS IX, pp. 93–104. doi:10.1145/378993.379006.
9. Li, Q.; De Rosa, M.; Rus, D. Distributed Algorithms for Guiding Navigation Across a Sensor Network. Proceedings of the 9th Annual International Conference on Mobile Computing and Networking; ACM: New York, NY, USA, 2003; MobiCom '03, pp. 313–325. doi:10.1145/938985.939017.
10. Li, Q.; Fang, Z.; Li, Q.; Zong, X. Multiobjective Evacuation Route Assignment Model Based on Genetic Algorithm. 2010 18th International Conference on Geoinformatics, 2010, pp. 1–5. doi:10.1109/GEOINFORMATICS.2010.5567485.
11. Holland, J.H. *Adaptation in Natural and Artificial Systems: An Introductory Analysis with Applications to Biology, Control and Artificial Intelligence*; MIT Press: Cambridge, MA, USA, 1992.
12. Gelenbe, E.; Liu, P.; LainLaine, J. Genetic Algorithms for Route Discovery. *IEEE Transactions on Systems, Man, and Cybernetics, Part B (Cybernetics)* **2006**, *36*, 1247–1254. doi:10.1109/TSMCB.2006.873213.
13. Yadegari, M. A Biologically-Inspired Optimization Algorithm For Urban Evacuation Planning In Disaster Management. 2010.
14. Ferscha, A.; Zia, K. LifeBelt: Crowd Evacuation Based on Vibro-Tactile Guidance. *IEEE Pervasive Computing* **2010**, *9*, 33–42. doi:10.1109/MPRV.2010.83.
15. Wong, S.K.; Wang, Y.S.; Tang, P.K.; Tsai, T.Y. Optimized Evacuation Route Based on Crowd Simulation. *Computational Visual Media* **2017**, *3*, 243–261. doi:10.1007/s41095-017-0081-9.
16. Filippoupolitis, A. Emergency Simulation and Decision Support Algorithms. PhD thesis, 2010.
17. Nowak, M.; Nowak, S.; Domańska, J.; Czachórski, T. Cognitive Packet Networks for the Secure Internet of Things. 2019 Global IoT Summit (GIoTS), 2019, pp. 1–4. doi:10.1109/GIOTS.2019.8766380.
18. Gorbil, G.; Gelenbe, E. Opportunistic Communications for Emergency Support Systems. *Procedia Computer Science* **2011**, *5*, 39–47. doi:10.1016/j.procs.2011.07.008.
19. Kinatader, M.; Comunale, B.; Warren, W.H. Exit Choice in an Emergency Evacuation Scenario Is Influenced by Exit Familiarity and Neighbor Behavior. *Safety Science* **2018**, *106*, 170–175. doi:10.1016/j.ssci.2018.03.015.
20. Chen, L.; Tang, T.Q.; Huang, H.J.; Song, Z. Elementary Students' Evacuation Route Choice in a Classroom: A Questionnaire-Based Method. *Physica A: Statistical Mechanics and its Applications* **2018**, *492*, 1066–1074. doi:10.1016/j.physa.2017.11.036.
21. Haghani, M.; Sarvi, M. Simulating Dynamics of Adaptive Exit-Choice Changing in Crowd Evacuations: Model Implementation and Behavioural Interpretations. *Transportation Research Part C: Emerging Technologies* **2019**, *103*, 56–82. doi:10.1016/j.trc.2019.04.009.
22. Zhong, J.; Cai, W.; Luo, L. Crowd Evacuation Planning Using Cartesian Genetic Programming and Agent-Based Crowd Modeling. 2016, Vol. 2016-February, *Proceedings - Winter Simulation Conference*, pp. 127–138. doi:10.1109/WSC.2015.7408158.
23. Lopez-Carmona, M.A. CelLEVAC: An Adaptive Guidance System for Crowd Evacuation through Behavioral Optimization. *arXiv:2007.05963 [cs, eess]* **2020**, [arXiv:cs, eess/2007.05963].
24. Zhong, J.; Luo, L.; Cai, W.; Lees, M. Automatic Rule Identification for Agent-Based Crowd Models through Gene Expression Programming. 2014, Vol. 2, *13th International Conference on Autonomous Agents and Multiagent Systems, AAMAS 2014*, pp. 1125–1132.



25. Miller, J. Cartesian Genetic Programming. *Cartesian Genetic Programming* **2011**.
26. Helbing, D.; Molnár, P. Social Force Model for Pedestrian Dynamics. *Physical Review E* **1995**, *51*, 4282–4286. doi:10.1103/PhysRevE.51.4282.
27. Fred Glover. *Tabu Search*; Kluwer Academic Publishers, 1997.
28. Lesani, A.; Nateghinia, E.; Miranda-Moreno, L.F. Development and Evaluation of a Real-Time Pedestrian Counting System for High-Volume Conditions Based on 2D LiDAR. *Transportation Research Part C: Emerging Technologies* **2020**, *114*, 20–35. doi:10.1016/j.trc.2020.01.018.
29. Kurkcu, A.; Ozbay, K. Estimating Pedestrian Densities, Wait Times, and Flows with Wi-Fi and Bluetooth Sensors. *Transportation Research Record* **2017**, *2644*, 72–82. doi:10.3141/2644-09.
30. Akhter, F.; Khadivizand, S.; Siddiquei, H.R.; Alahi, M.E.E.; Mukhopadhyay, S. IoT Enabled Intelligent Sensor Node for Smart City: Pedestrian Counting and Ambient Monitoring. *Sensors* **2019**, *19*, 3374. doi:10.3390/s19153374.
31. Ilyas, N.; Shahzad, A.; Kim, K. Convolutional-Neural Network-Based Image Crowd Counting: Review, Categorization, Analysis, and Performance Evaluation. *Sensors* **2020**, *20*, 43. doi:10.3390/s20010043.
32. Chen, Y.L.; Liu, D.; Wang, S.; Li, Y.F.; Zhang, X.S. Self-Powered Smart Active RFID Tag Integrated with Wearable Hybrid Nanogenerator. *Nano Energy* **2019**, *64*, 103911. doi:10.1016/j.nanoen.2019.103911.
33. Correa, A.; Barcelo, M.; Morell, A.; Vicario, J.L. A Review of Pedestrian Indoor Positioning Systems for Mass Market Applications. *Sensors* **2017**, *17*, 1927. doi:10.3390/s17081927.
34. Alvarez Lopez, Y.; de Cos Gomez, M.E.; Las-Heras Andres, F. A Received Signal Strength RFID-Based Indoor Location System. *Sensors and Actuators A: Physical* **2017**, *255*, 118–133. doi:10.1016/j.sna.2017.01.007.
35. Brchan, J.L.; Zhao, L.; Wu, J.; Williams, R.E.; Pérez, L.C. A Real-Time RFID Localization Experiment Using Propagation Models. 2012 IEEE International Conference on RFID (RFID), 2012, pp. 141–148. doi:10.1109/RFID.2012.6193042.
36. Assarian, A.; Khademzadeh, A.; Hosseinzadeh, M.; Setayeshi, S. An Efficient Resource Allocation Scheme in a Dense RFID Network Based on Cellular Learning Automata. *International Journal of Communication Systems* **2019**, *32*, e3835. doi:10.1002/dac.3835.
37. Duives, D.C.; Mahmassani, H.S. Exit Choice Decisions during Pedestrian Evacuations of Buildings. *Transportation Research Record* **2012**, *2316*, 84–94. doi:10.3141/2316-10.
38. Ortúzar, J.; Willumsen, L. *Modelling Transport*, fourth ed.; John Wiley and Sons: New York, 2011.
39. Rappaport, T.S. Wireless Communications – Principles and Practice, Second Edition. (The Book End). *Microwave Journal* **2002**, *45*, 128–129.
40. Xu, S.; Zhou, H.; Wu, C.; Huang, C.M.; Moon, S. Spatial Signal Attenuation Model of Active RFID Tags. *IEEE Access* **2018**, *6*, 6947–6960. doi:10.1109/ACCESS.2018.2794556.
41. Lopez-Carmona, M.A.; Marsa-Maestre, I.; de la Hoz, E. A Cooperative Framework for Mediated Group Decision Making. In *Modern Approaches to Agent-Based Complex Automated Negotiation*; Fujita, K.; Bai, Q.; Ito, T.; Zhang, M.; Ren, F.; Aydoğan, R.; Hadfi, R., Eds.; Springer International Publishing: Cham, 2017; pp. 35–50. doi:10.1007/978-3-319-51563-2.